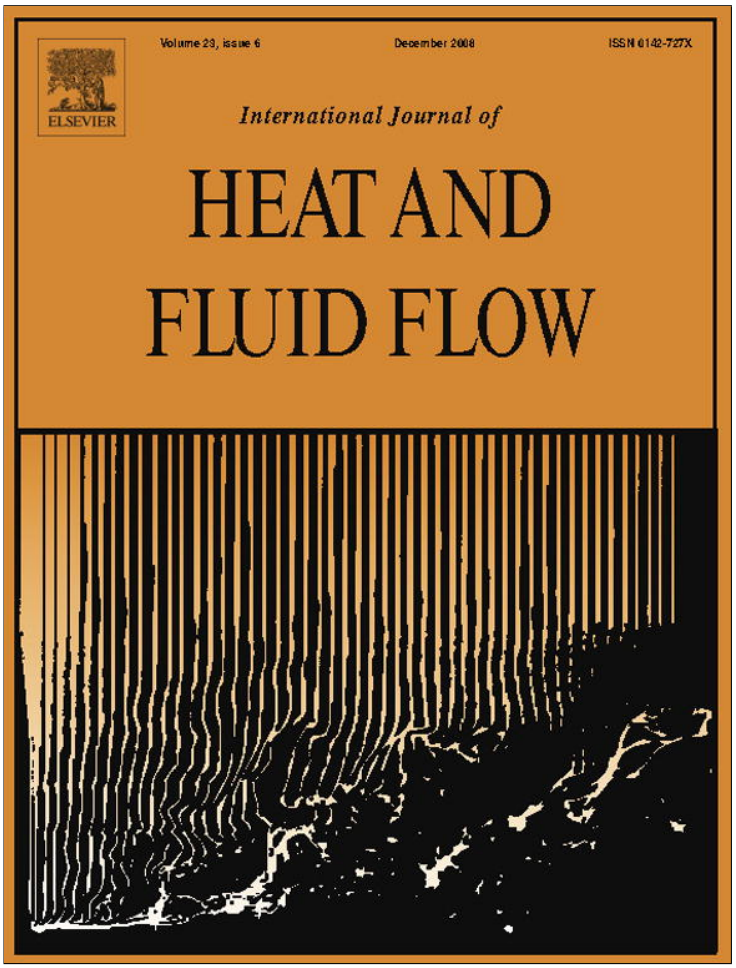

International Journal of Heat and Fluid Flow 29 (2008) 1638–1649

Contents lists available at ScienceDirect

International Journal of Heat and Fluid Flow

journal homepage: www.elsevier.com/locate/ijhff

# A hybrid RANS-LES approach with delayed-DES and wall-modelled LES capabilities

Mikhail L. Shur [a], Philippe R. Spalart [b], Mikhail Kh. Strelets [a,*], Andrey K. Travin [a]

[a] New Technologies and Services, 14, Dobrolyubov Avenue, 197198 St. Petersburg, Russia
[b] Boeing Commercial Airplanes, P.O. Box 3707, Seattle, WA 98124, USA

ARTICLE INFO

*Article history:*
Received 28 September 2007
Received in revised form 14 July 2008
Accepted 15 July 2008
Available online 9 September 2008

*Keywords:*
LES
Delayed detached-eddy simulation
Wall modelling in LES

ABSTRACT

A CFD strategy is proposed that combines delayed detached-eddy simulation (DDES) with an improved RANS-LES hybrid model aimed at wall modelling in LES (WMLES). The system ensures a different response depending on whether the simulation does or does not have inflow turbulent content. In the first case, it reduces to WMLES: most of the turbulence is resolved except near the wall. Empirical improvements to this model relative to the pure DES equations provide a great increase of the resolved turbulence activity near the wall and adjust the resolved logarithmic layer to the modelled one, thus resolving the issue of "log layer mismatch" which is common in DES and other WMLES methods. An essential new element here is a definition of the subgrid length-scale which depends not only on the grid spacings, but also on the wall distance. In the case without inflow turbulent content, the proposed model performs as DDES, i.e., it gives a pure RANS solution for attached flows and a DES-like solution for massively separated flows. The coordination of the two branches is carried out by a blending function. The promise of the model is supported by its satisfactory performance in all the three modes it was designed for, namely, in pure WMLES applications (channel flow in a wide Reynolds-number range and flow over a hydrofoil with trailing-edge separation), in a natural DDES application (an airfoil in deep stall), and in a flow where both branches of the model are active in different flow regions (a backward-facing-step flow).


## 1. Introduction

Recently, noticeable progress has been reached in building hybrid RANS-LES models for both high Reynolds number massively separated flows and more general cases that also include attached and mildly separated regions. For the former, probably the most popular approaches are detached-eddy simulation or DES (Spalart et al., 1997) hereafter referred to as DES97, and its recent modification, delayed DES or DDES (Spalart et al., 2006). A general feature of these two approaches is that the whole or at least a major part of the attached boundary layer is treated by RANS, while LES is applied only in the separated flow regions. In contrast, in a second group of RANS-LES hybrids, which offers wall-modelling in LES (WMLES) of high Reynolds number flows, RANS is used only in a much thinner near-wall region, in which the wall distance is much smaller than the boundary-layer thickness but is still potentially very large in wall units (Piomelli and Balaras, 2002). Along with this, similarly to DES97 and DDES, in the attached flow regions these models use "RANS grids", i.e., they employ highly anisotropic grids with very large ("unlimited" in wall units) grid spacing in the directions parallel to the wall while, immediately adjacent to the wall, the wall-normal spacing is about one wall unit. Unfortunately, most WMLES approaches in the literature are zonal, and include some "channel-friendly" steps, i.e., elements that are easily implemented in channel flow but whose applicability in more complex flows is debatable. Other than that, some proposed solutions use substantial outside information such as fields from wall-resolved LES or DNS runs (e.g., Davidson and Dahlstrom, 2005) or synthetic turbulence (e.g., Davidson and Billson, 2006) at the RANS-LES interface, and/or require averages in the wall-parallel directions to define intermediate quantities (e.g., Temmerman et al., 2005) or to avoid negative eddy viscosity and similar difficulties. Although rather successful in some cases, all these and other similar models are not completely formulated for cases where a complex geometry is involved.

Other approaches are closer to being generally applicable. The Limited Numerical Scales approach of Batten et al. (2002) shares the simplicity and non-zonal nature of DES97, is capable of natural DES, and was used for WMLES in a channel (Batten et al., 2004). It did better on a very coarse grid, with weak resolved stress, than in a more conventional situation with LES dominance of the outer layer. The WMLES approach of Abe (2005) has many similarities with the present one both in terms of purpose (although he is also focused on the normal Reynolds stresses, and does not shy away from very coarse grids, relative to channel width) and level of complexity. Its capability in natural DES mode is not mentioned in that paper, but the RANS model appears to have a standard $k$–$\varepsilon$

* Corresponding author.
*E-mail address:* strelets@mail.rcom.ru (M.Kh. Strelets).

0142-727X/$ - see front matter © 2008 Elsevier Inc. All rights reserved.
doi:10.1016/j.ijheatfluidflow.2008.07.001

behaviour and therefore should cover the entire boundary layer, provided the grid is not "ambiguous" as defined in Spalart et al. (2006).

The work of Schiestel and Dejoan (2005) is similar to ours in the sense that they also aim at the full range from RANS to LES, but again do not avoid grid densities we would view as ambiguous (and would therefore steer to RANS mode), and their derivation has a more theoretical flavour than ours. The SGS model used in this work depends on the entire resolved turbulent kinetic energy and length-scale, thus requiring averaging. This is not typical, and the importance of the grid spacing when it is very fine relative to the integral scale (that is, in a high-accuracy LES) is very obscure. Only one channel case is presented, and is free of log-layer mismatch per se, but the resolved Karman constant is abnormally high, near 0.55, possibly due to the large streamwise grid spacing, 0.2 of channel half-width. The wall-normal stretching is also very rapid in places.

Note that the DES formalism can also be used for WMLES, and this does not imply any additional complexity and/or impractical, "channel-friendly", steps. The first attempt to do this in the developed channel flow (Nikitin et al., 2000) turned out generally successful in the sense that the approach, indeed, enabled LES predictions at unlimited values of grid spacing parallel to the wall in wall units. The Reynolds-number dependence of the computing cost is logarithmic, rather than a power dependence as in wall-resolved LES. As could be expected, the simulations produced two logarithmic layers: the "inner" log-layer, which arises because the RANS model is constructed to provide it and the "outer" log-layer, which arises because LES is functioning well once all local grid-sizes are much smaller than the distance to the wall. Unfortunately, these two log-layers turn out mismatched (having different intercepts $C$) resulting in an under-prediction of the skin-friction by up to 15–20%, an error that is far too large to meet the demands of the aerospace industry. This flaw in DES is completely inherited by DDES; neither method has so far been adjusted to deal with the mismatch because WMLES was not their primary application.

Thus, there is a strong motivation to find a remedy of log-layer mismatch (LLM) within a non-zonal, DES-like approach. However, the ambition for the present work is not restricted to this: its objective is to build a single set of formulas both for natural (D)DES applications and for WMLES uses, so that different flows or (more importantly) different regions inside a single simulation over a complex geometry can each be automatically treated by a very capable model.

The rest of the paper is organized as follows. In Section 2 we present the formulation of the proposed model (hereafter it is referred to as Improved DDES or IDDES). Then, in Section 3, a series of tests is presented which include pure WMLES applications followed by a simulation of the backward-facing-step flow, in which both WMLES and DDES branches are active in different flow regions.

## 2. IDDES formulation

Provided that the DDES model is already available in a code, the implementation of the IDDES approach presented in this section is simple. However, in theoretical terms, the difference between the two models is not that minor. First of all, IDDES includes two branches, DDES and WMLES, and a set of empirical functions designed to obtain both correct performance from these branches themselves and their coupling ensuring a favourable response of the combined model as DDES or WMLES depending on the inflow (or initial) conditions used in the simulation. In this sense, there is an intentional non-uniqueness of the solution within given lateral boundary conditions; this feature originated with DDES, and the finding that a successful gradual shift from RANS to LES is unlikely.

A separate and essential element of the proposed model is a new definition of the subgrid length-scale that includes explicit wall-distance dependence, unlike the usual LES and DES practice, which involves only the grid-spacings. Below we outline all the elements of IDDES starting from this new subgrid length-scale, which enters both of its branches. The presentation assumes a structured near-orthogonal grid.

### 2.1. Subgrid length-scale

The issue of the optimal relation between the subgrid length-scale and grid-spacings is not specific to the model developed in the present work, but is a general issue of any LES approach not involving an explicit filtering. It is far from trivial, especially when the computational grid is significantly anisotropic, which is typical of the wall-bounded flows we are concerned with here. Almost all simulations of such flows use a finer spacing in the wall-normal direction than in the other two directions, and some also use finer spacing in the lateral direction than in the streamwise direction. With wall modelling, the wall-parallel spacings even become larger than the wall distance, thus violating the normal LES standard that the sub-grid eddies are all results of the energy cascade; this gives the SGS model much more leverage. Historically, the most widely employed definition has been the cube root of the cell volume. While this is a plausibly balanced quantity, it was challenged in DES literature (Spalart et al., 1997; Spalart, 2000), in which the maximum of the three cell dimensions was advocated instead (not based on any wall-proximity arguments). However, neither definition is successful, if judged by a straightforward application to wall-resolved LES of wall-bounded flows, with accepted gridding practices: the values of the SGS model constants which work well in free turbulent flows with cubic cells are then too large. For instance, the optimal value of the Smagorinsky constant for LES of channel flow is about 0.1 if the cube root is used, or roughly half its optimal value for Decaying Isotropic Homogeneous Turbulence (DIHT). Recall that the accepted criteria are very different, though: in DIHT it is the spectral slope near the spectral cut-off; in wall flows, it is the log-law intercept. Also recall the absence of a gap between energy-containing scales and the grid spacing. Using the maximum grid spacing, as in (D)DES, the difference between the optimal SGS model constants for DIHT and channel flow is even larger. This situation cannot be considered as a satisfactory one, not only because the two types of flows demand different constants but, more importantly, because any "wall-bounded" flow becomes a "free" one away from the walls, which means that the use of any single value of the constant calibrated on this or that type of flow cannot be correct in a whole flow. This motivates a search for an alternative and more physically justified definition of the subgrid length-scale, which would not demand different SGS model constants for wall-bounded and free turbulent flows.

Since wall-proximity effects, primarily inviscid blocking, are involved, it seems natural to allow such a definition to rely not only on the cell sizes, but also to explicitly include a wall-distance dependency, i.e., have the form:

$$\Delta = f(h_x, h_y, h_z, d_w), \tag{1}$$

where $\Delta$ is the needed subgrid length-scale, $h_x$, $h_y$, and $h_z$ are the local streamwise, wall-normal, and lateral cell sizes, respectively, and $d_w$ is the distance to the wall. Note that Abe (2005) also uses the wall distance, as well as the direction of the wall-normal, which is a more volatile quantity (but only up to about $y^+ = 250$).

Let $\Delta_{free}$ be the limit of the function $f(h_x, h_y, h_z, d_w)$ for infinite $d_w$. Then, following the DES papers and the argument of statistical isot-

ropy of the small eddies, it is set equal to the maximum local grid spacing

$$\Delta_{\text{free}} = h_{\max} \equiv \max\{h_x, h_y, h_z\}. \tag{2}$$

Note however that away from the walls, the grid for an LES should be fairly isotropic anyway (in other words, a spacing much below $h_{\max}$ in any direction is wasted), and so the impact of this specific choice is not crucial. This function is, appropriately, insensitive to the wall-normal direction.

As for the behaviour of $\Delta$ in very close vicinity of the wall, it should not completely follow the drastic decrease of the wall-normal step typical of this region (especially at high Reynolds number) and, therefore, should depend on the wall-parallel steps only:

$$\Delta_{\text{wall}} = \Delta(h_x, h_z) \tag{3}$$

Assuming, finally, that between these two limiting cases $\Delta$ is a linear function of $d_w$ and that at any distance from the wall it varies within the range $h_{\min} \leqslant \Delta \leqslant h_{\max}$, a definition of the subgrid length-scale satisfying all the above demands is as follows:

$$\Delta = \min\{\max[C_w d_w, C_w h_{\max}, h_{wn}], h_{\max}\}, \tag{4}$$

where $h_{wn}$ is the grid step in the wall-normal direction and $C_w$ is an empirical constant, which does not depend on the specific SGS model. Its value was set equal to 0.15 based on a wall-resolved LES of channel flow with the Smagorinsky SGS model, as seen shortly (Section 3.2), and then the same value of the constant was used with other SGS models.

Fig. 1 shows two possible types of variation of the subgrid length-scale $\Delta$ defined by (4), normalized by the maximum grid step (i.e., the DES value), across a plane channel with half-width $H$. The first type (solid line in Fig. 1) takes place if $h_{wn} \leqslant C_w d_w$ and, therefore, in accordance with (4), as long as $d_w < h_{\max}$, the length-scale $\Delta$ remains constant equal to $C_w h_{\max}$. Then, once $d_w > h_{\max}$, it grows linearly ($\Delta = C_w d_w$) until reaching the value of $h_{\max}$, and stays constant after that. The second type of $\Delta$ variation (dashed line in Fig. 1) corresponds to a strong wall-normal step stretching. This branch is introduced to avoid a violation of the physical constraint $\Delta \geqslant h_{\min}$ mentioned above. In this case, $\Delta$ remains constant and equal to $C_w h_{\max}$ as long as $h_{wn} < C_w h_{\max}$. Then, it grows with a rate higher than $C_w$ until reaching the value of $h_{\max}$ and after that, just as in the first case, remains constant. Note that this scenario is undesirable, but with any rate of wall-normal step stretching that is acceptable for an accurate LES, it still does not lead to disaster. For instance, for a wall-normal step varying in accordance with a geometric series, it takes place only if the series index $k > (1 + C_w)$, i.e., if $k > 1.15$, which is close to the maximum $k$ values (1.2–1.3) that still provide sufficient accuracy in LES. Therefore, with any acceptable rate of growth of the wall-normal step, the difference between the two branches of (4) is not large.

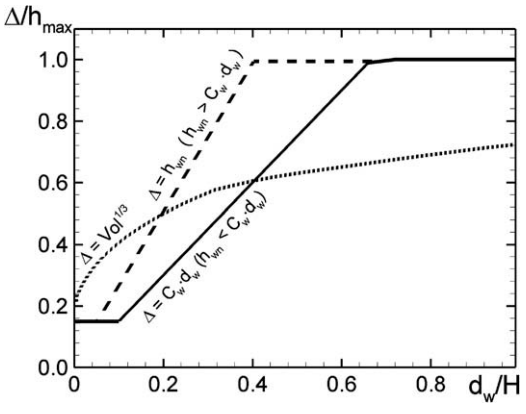


**Fig. 1.** Two types of variation of the subgrid length-scale (4) across plane channel compared to variation of the scale based on cube root of cell volume (dotted line).

The primary effect of (4) is to reduce $\Delta$, and also to give it a fairly steep variation, leading to a similar trend in the eddy viscosity (especially with the Smagorinsky model, as opposed to transport-equation models), which is likely to de-stabilize the flow. This is helpful, as discussed again later. Note that the cube root definition also reduces $\Delta$ near the wall, but not linearly (see dotted line in Fig. 1).

Examples demonstrating the convincing performance of the subgrid length-scale (4) in the framework of different LES and hybrid RANS-LES approaches are presented in Section 3.

### 2.2. DDES branch of IDDES

This branch is responsible for the DDES-like functionality of IDDES and should become active only when the inflow conditions do not have any turbulent content (if a simulation has spatial periodicity, the initial conditions rather than the inflow conditions set the character of the simulation) and in particular when a grid of "boundary-layer type" precludes the resolution of the dominant eddies. Recall that the DDES formulation (Spalart et al., 2006) reads as

$$l_{\text{DDES}} = l_{\text{RANS}} - f_d \max\{0, (l_{\text{RANS}} - l_{\text{LES}})\} \tag{5}$$

Here the delaying function, $f_d$, is defined as $f_d = 1 - \tanh[(8r_d)^3]$, and the quantity $r_d$ borrowed from the SA RANS turbulence model (Spalart and Allmaras, 1994),

$$r_d = \frac{\nu + \nu_t}{\kappa^2 d_w^2 \cdot \max\{[\sum_{ij}(\partial u_i/\partial x_j)^2]^{1/2}, 10^{-10}\}}, \tag{6}$$

is a marker of the wall region equal to 1 in a log layer and 0 in a free shear flow.

In accordance with the general DES concept, in order to create a seamless hybrid model, the length-scale $l_{\text{DDES}}$ defined by (5) is substituted into the background RANS model in place of the RANS length-scale, $l_{\text{RANS}}$, explicitly or implicitly involved in any such model. For instance, for the SA model the length-scale is equal to the distance to the wall $l_{\text{RANS}} = d_w$, while the $k$–$\omega$ MSST model (Menter, 1993) has $l_{\text{RANS}} = k^{1/2}/(C_\mu \omega)$. In the original DES, the length-scale depends only on the grid. In DDES and here, it also depends on the solution, via (5) and (6).

As far as the LES length-scale, $l_{\text{LES}}$, in (5) is concerned, it is defined via the subgrid length-scale $\Delta$ (4) as

$$l_{\text{LES}} = C_{\text{DES}} \Psi \Delta, \tag{7}$$

where $C_{\text{DES}}$ is the fundamental empirical constant of DES (Shur et al., 1999) and $\Psi$ is a low-Reynolds number correction (see Spalart et al., 2006) introduced in order to compensate the activation of the low-Reynolds number terms of some background RANS model in LES mode. Both $C_{\text{DES}}$ and $\Psi$ depend on the background RANS model, and the latter is equal to 1 if the RANS model does not include any low-Reynolds number terms (e.g., the MSST model). For the SA model this function reads:

$$\Psi^2 = \min\left[10^2, \frac{1 - \frac{c_{b1}}{c_{w1}\kappa^2 f_w^*}[f_{t2} + (1 - f_{t2})f_{v2}]}{f_{v1}\max(10^{-10}, 1 - f_{t2})}\right],$$

where all the notations, except for the quantity $f_w^*$, are the same as in the SA RANS model and $f_w^* = 0.424$. This, again, depends on the solution since the $f$-functions depend on the eddy-viscosity.

Considering that the quantity $r_d$ defined by (6) is close to 1.0 in the logarithmic part of the turbulent boundary layer (Spalart and Allmaras, 1994), the delaying function $f_d$ in (5) turns out to be close to zero there. As a result, the definition of length-scale (5), in contrast to the original definition used in DES (Spalart et al., 1997),

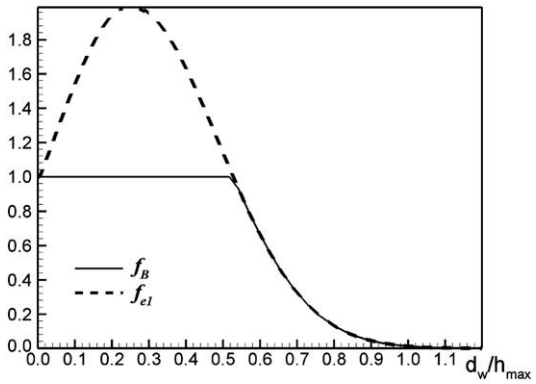


**Fig. 2.** Profiles of functions $f_B$ and $f_{e1}$ in plane channel.

ensures DDES performance in its RANS mode in the major part of any attached boundary layer independently on the wall-parallel grid-spacings, thus eliminating the known incorrect DES performance on "ambiguous" grids (Spalart et al., 2006). At the same time, outside this region, $r_d$ is small, $f_d$ is close to 1, and the model reduces to the original DES97. However, as emphasized by Spalart et al. (2006) and mentioned in the Introduction, when used as a wall model in LES, DDES does not have any advantages over the DES97.

### 2.3. WMLES branch of IDDES

This branch is intended to be active only when the inflow conditions used in the simulation are unsteady and impose some turbulent content[1] and the grid is fine enough to resolve boundary-layer dominant eddies. It presents a new seamless hybrid RANS-LES model, which couples RANS and LES approaches via the introduction of the following blended RANS-LES length-scale:

$$l_{WMLES} = f_B(1+f_e)l_{RANS} + (1-f_B)l_{LES}, \tag{8}$$

where, similarly to DDES, $l_{RANS}$ and $l_{LES}$ are the RANS and LES length-scales, respectively.

Let us now consider the two other ingredients of the length-scale (8), namely, the functions $f_B$ and $f_e$.

The empirical blending-function $f_B$ depends upon $d_w/h_{max}$ and is defined as

$$f_B = \min\{2\exp(-9\alpha^2), 1.0\}, \quad \alpha = 0.25 - d_w/h_{max}. \tag{9}$$

It varies from 0 to 1 and provides rapid switching of the model from RANS mode ($f_B = 1.0$) to LES mode ($f_B = 0$) within the range of wall-distance $0.5h_{max} < d_w < h_{max}$ (see solid line in Fig. 2). Again, the intent is for the dynamics not to linger between RANS and LES mode.

The second empirical function involved in (8), elevating-function $f_e$, is aimed at preventing the excessive reduction of the RANS Reynolds stresses which has been observed in the interaction of the RANS and LES regions in the vicinity of their interface. It is instrumental in combating log-layer mismatch. The function $f_e$ should be close to zero, and therefore passive, in two cases:

(1) when the grid used in the simulation is sufficient for a wall-resolved LES (the RANS-LES interface is located very close to the wall, at $y^+ < 15$–$20$, so that the Reynolds stresses near the interface are negligible);
(2) when the final IDDES model (see Eq. (17) in Section 2.4 below) effectively performs as the background RANS model (otherwise, a non-zero $f_e$ would corrupt the correct RANS behaviour).

The function built to satisfy these two demands but have an effect when needed reads:

$$f_e = \max\{(f_{e1}-1), 0\}\Psi f_{e2}. \tag{10}$$

Here the function $f_{e1}$ is defined as

$$f_{e1}(d_w/h_{max}) = \begin{cases} 2\exp(-11.09\alpha^2) & \text{if} \quad \alpha \geqslant 0 \\ 2\exp(-9.0\alpha^2) & \text{if} \quad \alpha < 0 \end{cases}. \tag{11}$$

It provides a "predefined" (i.e., dependent on the grid but not on the solution) "elevating" device for the RANS component of the WMLES length-scale (8). As seen in Fig. 2, where $f_{e1}$ is shown by a dashed line, it coincides with $f_B$ when $f_B < 1$, i.e., in the RANS-LES switching region, but then, with $d_w$ decreasing, grows up to 2.0, and then gradually falls back to 1.0 at the wall.

The function $f_{e2}$ in (10) reads:

$$f_{e2} = 1.0 - \max\{f_t, f_l\}. \tag{12}$$

It controls the intensity of "elevating" of the RANS component of the model (8) through the following two functions:

$$f_t = \tanh[(c_t^2 r_{dt})^3], \quad f_l = \tanh[(c_l^2 r_{dl})^{10}], \tag{13}$$

where the quantities $r_{dt}$ and $r_{dl}$ are the "turbulent" and "laminar" analogues of $r_d$ (6) defined by the relations

$$\begin{cases} r_{dt} = \dfrac{\nu_t}{\kappa^2 d_w^2 \cdot \max\left\{\left[\sum_{ij}(\partial u_i/\partial x_j)^2\right]^{1/2}, 10^{-10}\right\}}, \\ r_{dl} = \dfrac{\nu}{\kappa^2 d_w^2 \cdot \max\left\{\left[\sum_{ij}(\partial u_i/\partial x_j)^2\right]^{1/2}, 10^{-10}\right\}}, \end{cases} \tag{14}$$

and $c_t$ and $c_l$ are additional model constants which depend on the background RANS turbulence model and should be adjusted so that the function $f_{e2}$ is virtually zero when either $r_{dt}$ or $r_{dl}$ is close to 1.0.

Similar to the parameter $r_d$, $r_{dt}$ is close to 1.0 in the logarithmic part of the boundary layer, while the new parameter, $r_{dl}$, is close to 1.0 in the laminar sublayer. Thus, with properly chosen constants, inside the boundary layer one of the functions $f_t$ or $f_l$ in (13) is also close to 1.0, and therefore, $f_{e2}$ and $f_e$ are close to zero which ensures satisfaction of the demands (1) and (2) formulated above.

Note in conclusion that, in contrast to $f_{e1}$, $f_{e2}$ depends on the solution via the quantity $\sum_{ij}(\partial u_i/\partial x_j)^2$ in the denominator of $r_{dt}$ and $r_{dl}$. Such distinctions have become familiar starting with DDES. As for the introduction of the function $\Psi$ into the definition of $f_e$ (10), it is unrelated to the low-Re correction role this function plays in the LES mode of (D)DES, and is purely empirical. A better function to enforce the effect of $f_e$ when the background RANS model has the low-Re terms could probably be devised. However, as shown in the next section, even with this choice, the IDDES performance turns out quite satisfactory, so that the search for another function is not crucial.

### 2.4. Blending of DDES and WMLES branches

The DDES length-scale (5) and that of the WMLES-branch (8) do not blend directly in a way which ensures an automatic choice of the WMLES or DDES mode by the combined model we want to build, depending on the type of the simulation (with or without turbulent content) and the grid used. However this is possible with a modified version of (5) effectively equivalent to the original one in DDES (5), namely,

$$\tilde{l}_{DDES} = \tilde{f}_d l_{RANS} + (1-\tilde{f}_d)l_{LES}, \tag{15}$$

[1] For flows periodic in the streamwise direction, this turbulent content is imposed via the initial fields rather than the inflow condition (see Section 3.2).

where the blending function $\tilde{f}_d$ is defined by

$$\tilde{f}_d = \max\{(1 - f_{dt}), f_B\} \tag{16}$$

with $f_{dt} = 1 - \tanh[(8r_{dt})^3]$.

With the use of (15), the required IDDES length-scale combining the DDES and WMLES scales (15) and (8) is straightforward and can be implemented as

$$l_{hyb} = \tilde{f}_d(1 + f_e)l_{RANS} + (1 - \tilde{f}_d)l_{LES}. \tag{17}$$

Indeed, in the simulations with an inflow turbulent content: $r_{dt} \ll 1$; $f_{dt}$ is close to 1.0; $\tilde{f}_d$ defined by (16) is equal to $f_B$; and so (17) automatically reduces to $l_{hyb} = l_{WMLES}$ (8). Otherwise, as discussed in Section 2.3, $f_e$ becomes zero, and (17) reduces to $l_{hyb} = \tilde{l}_{DDES}$ (15). This behaviour of the length-scale (17) is supported by the numerical tests presented below.

This section reflects the unfortunate trend, from DES97 through DDES and on to IDDES, of increasing complexity. It is possible a simpler system with the same performance will be found in the future; a detailed publication now, especially since the approach is in use by at least two other groups (see Piomelli et al. (2007) and Mockett et al. (2007)), appears a useful step for better proposals to arise from the community. It is also important to have a complete and durable record of any method.

## 3. IDDES tests

### 3.1. Overview

Two examples are first given demonstrating the favourable performance of the subgrid length-scale (4) in the framework of wall-resolved LES of flow in a plane channel at a low Reynolds number, and within WMLES of this flow at a high Reynolds number. These examples are aimed at supporting the claim that this length-scale alone allows accurate LES of wall-bounded flows with the Smagorinsky model, without any adjustment of the subgrid model constant calibrated in DIHT.

A series of tests is then presented aimed at demonstrating the capabilities of the LES length-scale (4) imbedded into IDDES, i.e., into the hybrid RANS-LES length-scale (17). In order to evaluate IDDES performance in WMLES mode, it is applied to channel flow in a wide range of Reynolds number and to the flow over a hydrofoil with a shallow separation over an asymmetric trailing edge (experiment of Blake (1975)). After that, simulations are performed of the backward-facing step flow of Vogel and Eaton (1985), which allows evaluating IDDES in a mixed, DDES-WMLES, mode. One more test (not shown) confirming that for massively separated flows IDDES performs quite the same as DES97 and DDES is the flow past NACA0021 airfoil in deep stall studied experimentally by Swalwell (2005).

All the test cases were computed with the use of two versions of IDDES (based on the SA and MSST background RANS models), which can be readily obtained by substitution of the length-scale (17) in place of the distance to the wall $d_w$ in the destruction term of the SA eddy-viscosity transport equation, or in place of the length $l_{MSST} = k^{1/2}/(C_\mu\omega)$ in the dissipation term of the $k$-transport equation of the MSST model. The values of the empirical constants $c_l$ and $c_t$ involved in the definition of the WMLES length-scale (8) were adjusted based on preliminary simulations of channel flow. They are 3.55 and 1.63 for the SA and 5.0 and 1.87 for the MSST versions, respectively.

The simulations were carried out with the use of the incompressible branch of the NTS code (Strelets, 2001). The code uses the implicit scheme of Rogers and Kwak (1988). Time-derivatives are approximated with 2nd order backward differences (three-layer scheme) with dual time-stepping (infinite default pseudo-time step) and subiterations. The number of subiterations at each time step depends on the problem but usually is within the range from 5 to 20 (this ensures reduction of the maximum residual by 3–4 orders of magnitude). The time implicit scheme is implemented with the use of Gauss–Seidel relaxation by planes. For the spatial approximation of the inviscid fluxes, the code provides different options. In this work we use 4th-order centered approximation for the channel and hydrofoil flows and a weighted, 5th order upwind/4th order centered, scheme with a blending function dependent on the solution (Strelets, 2001; Travin et al., 2002) for the stalled airfoil and backward-facing step flows. The viscous terms in the equations are approximated with the 2nd-order centered scheme.

### 3.2. Demonstration of the advantages of the subgrid length-scale (4)

To support the advantage of the proposed subgrid LES length-scale (4) even in a wall-resolved LES, a simulation was carried out for a plane channel at $Re_\tau = 400$ with the use of the Smagorinsky SGS model with the wall-damping function of Piomelli et al. (1988):

$$\nu_t = (C_{SMAG}\Delta)^2\{1 - \exp[-(y^+/25)^3]\}S, \tag{18}$$

where $S$ is the magnitude of the strain tensor, $\Delta$ is the subgrid length-scale defined by (4), and $C_{SMAG}$ is set equal to 0.2, i.e., to the value established by Shur et al., 1999 based on LES of the DIHT flow in the NTS code, with the objective of maintaining a $-5/3$ spectral slope near the cut-off.

The grid is as follows: $\Delta x/H = 0.1$, $\Delta z/H = 0.05$, ($\Delta_x^+ = 40$, $\Delta_z^+ = 20$), the near-wall $y$-step is $\Delta y_1/H = 2 \times 10^{-3}$ ($\Delta y_1^+ = 0.8$), and the stretching factor of the wall-normal step is $k = 1.14$. The size of the computational domain is: $L_x = 8H$, $L_z = 3H$. The time step is 0.57, in wall units.

Fig. 3 shows that the mean velocity profile obtained in the simulation agrees very well with the DNS data of Moser et al. (1999). In contrast to this, with the traditional definition of the subgrid length-scale $\Delta$ via the cube root of the cell volume, the simulation carried out at $C_{SMAG} = 0.2$ gives much worse a solution (see dash-dot curve in Fig. 3). The resolved turbulence is severely damped. Similar (actually even worse) results were obtained at this value of the constant with the length-scale defined through the maximum grid-spacing.

The second example illustrating the advantage of the length-scale (4) is a WMLES of the high Reynolds number ($Re_\tau = 18{,}000$) channel flow. The simulation uses a DES-like WMLES method, which couples the Prandtl–van Driest RANS and the Smagorinsky SGS models:

$$\nu_t = \min\{(\kappa y)^2, (C_{SMAG}\Delta)^2\}\{1 - \exp[-(y^+/25)^3]\}S. \tag{19}$$

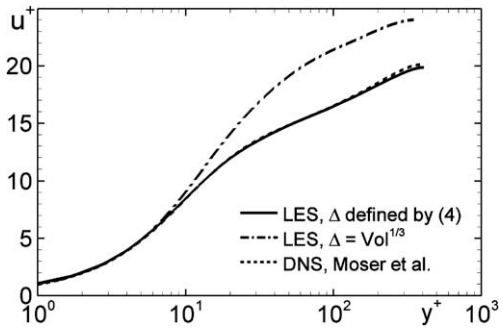


**Fig. 3.** Comparison of mean velocity profile from Smagorinsky LES of developed channel flow at $Re_\tau = 400$ with $\Delta$ defined by (4) and as cube root of cell volume with DNS of Moser et al. (1999).

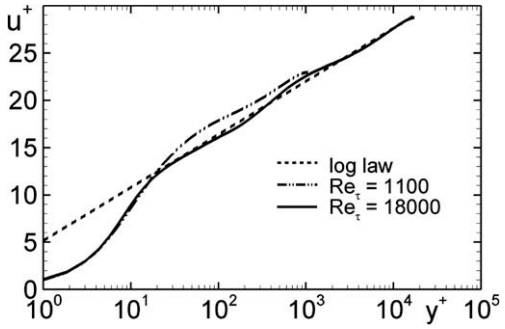


**Fig. 4.** Mean velocity profiles in developed channel flow computed with the use of DES model (19) and subgrid length-scale defined by (4) at $Re_\tau = 1100$ and 18,000.

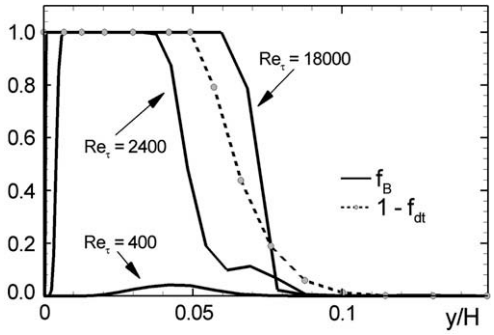


**Fig. 5.** Profiles of the functions $\tilde{f}_d$ and $(1 - f_{dt})$ in developed channel flow at different $Re_\tau$ from simulations with MSST version of IDDES and presence of initial turbulence content.

The grid in the wall-parallel directions is the same as that used in the previous example, normalized with channel width. The model switches from RANS to LES at $y/H = 0.0073$, $y^+ = 132$, where the eddy viscosity is about 40 times the molecular viscosity. The wall-normal grid has the same stretching factor, but the near-wall step is reduced to keep the value of $y_1^+$ less than 1.0. As seen in Fig. 4, the computed mean velocity profile at this Reynolds number (solid line in the figure) does not have any LLM and reproduces the log law fairly well.

Thus the two above examples confirm that the use of the subgrid length-scale (4) indeed results in quite accurate wall-resolved LES and high-Reynolds number DES of channel flow with the value of the Smagorinsky constant 0.2, compatible with the calibration on the DIHT flow. However this length-scale alone is still insufficient for accurate enough prediction of this flow at moderate Reynolds numbers (see the velocity profile at $Re_\tau = 1100$ shown in Fig. 4 by dash-dot line). Extra empiricism would be needed in (19). As shown in the next section, this issue is successfully resolved by IDDES, which provides uniformly accurate prediction of the channel flow at arbitrary Reynolds number.

### 3.3. IDDES testing in plane channel flow

This test is, in fact, the key one, since it is aimed at the evaluation of the new model's performance as applied to attached flows, i.e., to those, in which neither the original DES97 nor DDES, in their derivative use as WMLES, is capable of ensuring the level of accuracy expected in simple flows nowadays.

The series of simulations performed includes a $Re_\tau$ variation in the range from 400 up to 18,000. The latter value is large enough to predict the behaviour at arbitrarily high Reynolds number. The computational domain and the grid in the wall-parallel directions used in these simulations are the same as those used for the wall-resolved Smagorinsky LES at $Re_\tau = 400$ considered in the previous section. Thus, the series allows an assessment of the WMLES capability of IDDES on grids with very large ("unlimited") values of the wall-parallel grid steps in wall units, $\Delta x^+$ and $\Delta z^+$. The wall-normal grid is built in a conventional manner. Namely, the near-wall step is adjusted to the Reynolds number, to provide a value of $y_1^+$ below 1.0. Then, the grid step increases with a stretching factor 1.14. In accordance with (4), with this wall-normal step distribution, the first type of variation of the subgrid length-scale $\Delta$ across the channel (the solid line in Fig. 1) takes place.

Below we present results of the simulations obtained with the use of the MSST version of IDDES; results obtained with the SA version are quite similar.

As emphasized in Section 2, the behaviour of IDDES depends on whether the flow does or does not start with turbulent content. Let us first consider the first scenario (with turbulent content) which has been implemented via initialisation of the simulations with flow-fields obtained from LES of the DIHT flow with the use of the subgrid version of the MSST model (Strelets, 2001; Travin et al., 2002) as described in Spalart et al. (2006). The simulation recovers from a quite unrealistic initial field.

Fig. 5 shows profiles of the two branches of the blending function $\tilde{f}_d$ (16), $(1 - f_{dt})$ and $f_B$, computed at different values of $Re_\tau$ (recall that in all the simulations $h_{max} = 0.1$ in units of channel half-width $H$). One can see that at low and moderate $Re_\tau$, $f_B > (1 - f_{dt})$, and therefore, in accordance with (16), the $f_B$-branch of $\tilde{f}_d$ is active automatically providing a reduction of the hybrid length-scale (17) to the WMLES length-scale (8). At the high value of $Re_\tau = 18{,}000$, both branches of $\tilde{f}_d$ are active, the $(1 - f_{dt})$-branch prevailing near the wall and the $f_B$-branch dominating in the outer part of the RANS region. However, in this case they are close to each other, and so the specific choice of branch is not important.

As far as the behaviour of the elevating function $f_e$ is concerned, as seen in Fig. 6, in accordance with its design, it deviates from zero only in the RANS region. The deviation is most pronounced at moderate $Re_\tau$ and thus, the most significant strengthening of the RANS mode of the WMLES model is ensured exactly at these conditions; since the maximum value is less than 0.25, this can be considered a mild correction. This is demonstrated by profiles of the ratio of the hybrid to the RANS turbulent lengths-scale, $l_{hyb}/l_{RANS}$, at different $Re_\tau$ also plotted in Fig. 6. Consistently with the behaviour of $f_e$, the ratio is higher than 1.0 in the outer part of the RANS region (see Fig. 5) and is maximal at $Re_\tau = 1100$. This means a decreased level of turbulence dissipation relative to the original MSST RANS model, which prevents too strong a decrease of the eddy viscosity in this region and the unwanted rise of the modelled logarithmic

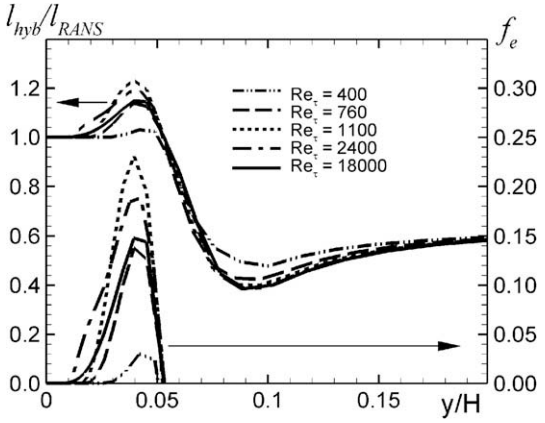


**Fig. 6.** Profiles of the function $f_e$ and ratio of length-scales of MSST-based IDDES and MSST RANS models in developed channel flow at different $Re_\tau$.

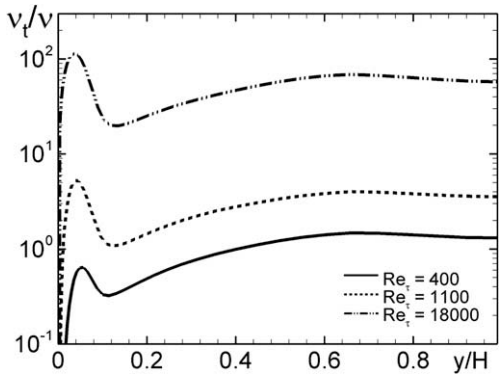


**Fig. 7.** Profiles of IDDES eddy viscosity normalized by molecular viscosity in developed channel flow at different $Re_\tau$.

layer. Then, in the LES region, the ratio drops abruptly, reaches a local minimum, and after that stays nearly constant equal to 0.6 with the present grid. The steep drop of the length-scale is an important feature of the proposed model, which makes its performance quite different from both DES97 and DDES, where it decreases more slowly. It results in a similar decrease of the eddy viscosity (see Fig. 7), which, in turn, helps to unlock the flow instabilities and activate turbulence with no artificial stirring.

The advantages of IDDES are clearly seen in a direct comparison of the flow visualizations from the simulations with the use of this model and MSST-based DDES presented in Fig. 8. The figure shows that IDDES does capture the major known features of the turbulence in the channel reasonably well. In particular, it does not allow the formation of smooth nearly one-dimensional eddies and excessive damping of turbulence at the RANS-LES interface, the way DES97 (Piomelli and Balaras, 2002) and DDES do. DDES fails, specifically, near the wall, whereas the two models behave very similarly near the center of the channel.

A quantitative assessment of the performance of MSST-based IDDES as applied to channel flow can be done based on Fig. 9, where we present the mean velocity profiles and resolved and modelled parts of the Reynolds shear stresses at different $Re_\tau$. DNS solutions at high Reynolds numbers being unavailable, the velocity profiles are compared with the Reichardt correlation (Reichardt, 1951):

$$U^+ = \frac{1}{\kappa}\ln(1.0 + 0.4y^+) + 7.8\left[1 - \exp\left(-\frac{y^+}{11}\right) - \left(\frac{y^+}{11}\right)\exp\left(-\frac{y^+}{3}\right)\right],$$

which achieves fairly good agreement with the DNS data at lower Reynolds numbers (e.g. Moser et al., 1999) and satisfies the defect law, making it a good benchmark. Note that IDDES performs well not only at the large $Re_\tau$, which is arguably an easier case for WMLES (see Piomelli et al. (1988); compare also the velocity profiles at $Re_\tau$ = 18,000 and 1100 in Fig. 4 above), but also at moderate and even low $Re_\tau$ corresponding to wall-resolved LES. This success will carry over to other wall-bounded flows, provided the wall-parallel grid is fine enough; note that the values used here, $\Delta x/H = 0.1$, $\Delta z/H = 0.05$, are economical.

Finally, Fig. 10 presents a direct comparison of the mean flow velocity and resolved and modelled parts of the Reynolds shear stress predicted by the MSST-based version of IDDES with the MSST-based DDES at $Re_\tau$ = 2400. It shows that IDDES leads to a significant increase of the resolved part of the stress, and to a complete elimination of the LLM. The diagonal Reynolds stresses (not shown) are also considerably improved. The increase in resolved turbulence, in other words the much deeper reach of LES towards the wall, is very likely to improve accuracy in non-trivial flows, for instance with pressure gradients.

To conclude the discussion of simulations of channel flow with the use of IDDES operating in WMLES mode, recall that all the results presented above were obtained on grids with the streamwise

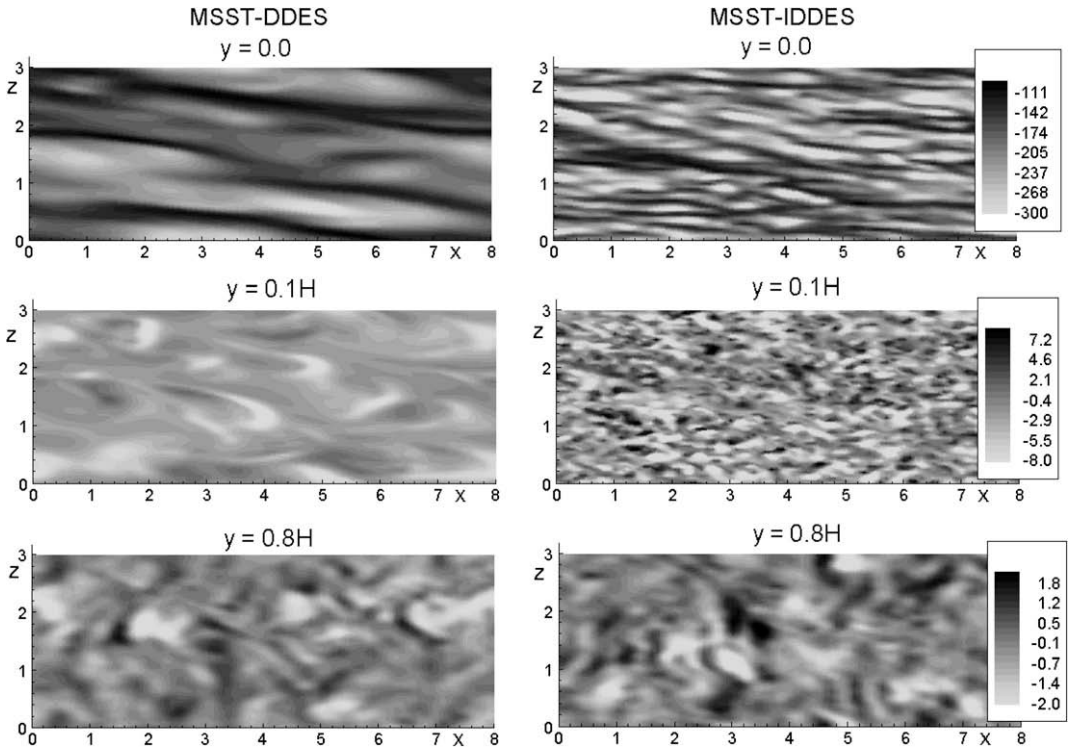


**Fig. 8.** Comparison of *XZ*-cuts of instantaneous vorticity magnitude from simulation of channel flow with MSST-based IDDES and MSST-based DDES at $Re_\tau$ = 2400.

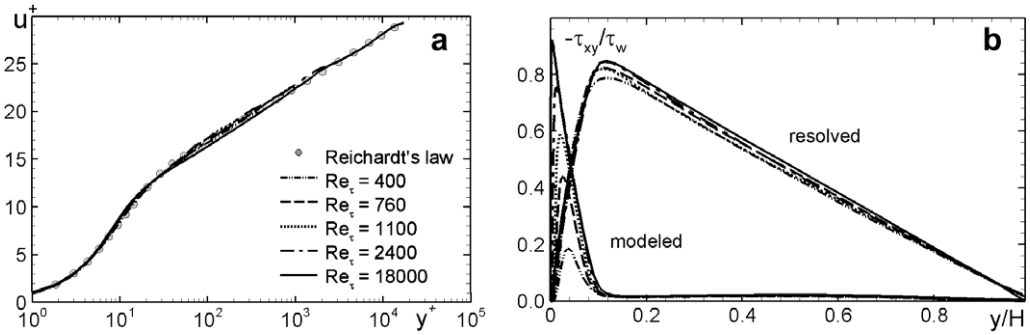


**Fig. 9.** Profiles of mean velocity (a) and resolved and modelled shear stresses (b) from MSST-based IDDES of channel flow at different $Re_\tau$.

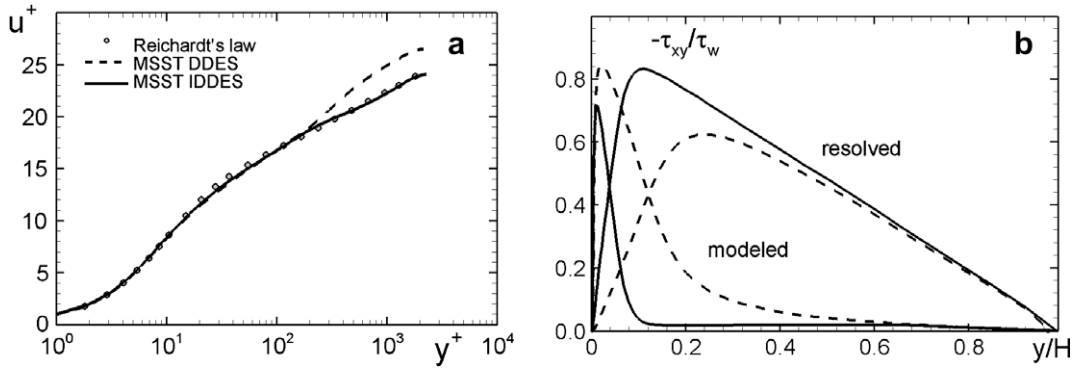


**Fig. 10.** Comparison of predictions of developed channel flow at $Re_\tau = 2400$ with MSST-based IDDES and MSST-based DDES.

step, $\Delta x$, twice as large as the spanwise step, $\Delta z$. Although this is common LES practice motivated by the knowledge of the turbulence structure in the channel and the flow direction, this is not practical for more complex flows, and so it is of interest to evaluate the reaction of the model to an alteration of the $\Delta x/\Delta z$ value. It is illustrated by Fig. 11, where the results of the simulation with $\Delta x/\Delta z = 2$ are compared with those with $\Delta x/\Delta z = 1.0$ and 4.0, $\Delta z$ being kept constant. The value 1.0 is much more likely in engineering practice, since the direction of the flow, especially very near the wall, is not known at the grid-design stage. One can see that, as expected, an increase of $\Delta x$ results in a growth of the modelled and decrease of the resolved parts of the shear stresses. Nonetheless, in the considered range of $\Delta x/\Delta z$ this does not cause a significant alteration of the total shear stress and the mean velocity profile. Therefore, the dependence chosen on $\Delta x$ and $\Delta z$ individually appears quite successful.

Let us now consider the performance of IDDES in the same flow but with no initial turbulent content. This situation is implemented by starting the simulations from a steady MSST RANS solution. In this case, independently of the Reynolds number, the solution returned by IDDES is identical to the initial RANS solution, which is exactly the behaviour that should be observed in accordance with the design of IDDES. The results do not depend on the wall-parallel grid spacing at all. This is seen in Fig. 12, where the velocity profiles are plotted from the simulations with the use of MSST-based IDDES and RANS. The figure also shows profiles of the functions $f_l$ and $f_t$, which help to understand the reason for this performance. One can see that at any $y^+$ one of the functions (either $f_l$ or $f_t$) is equal to 1.0, which results in the zeroing of $f_{e2}$ (see (12)) and, therefore, of $f_e$ as well (see (10)). Thus, in the situation considered (no turbulent content) IDDES actually reduces to a DDES-like model (15) and behaves exactly as DDES does in this situation, i.e., returns the

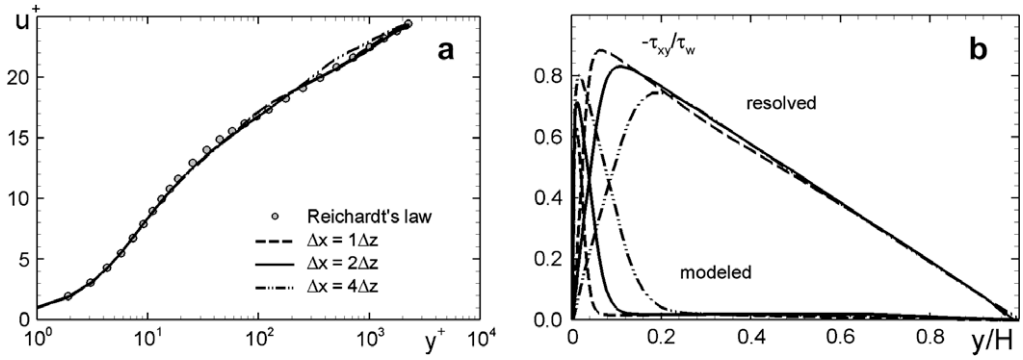


**Fig. 11.** Effect of streamwise grid step on prediction of developed channel flow at $Re_\tau = 2400$ with MSST-based IDDES.

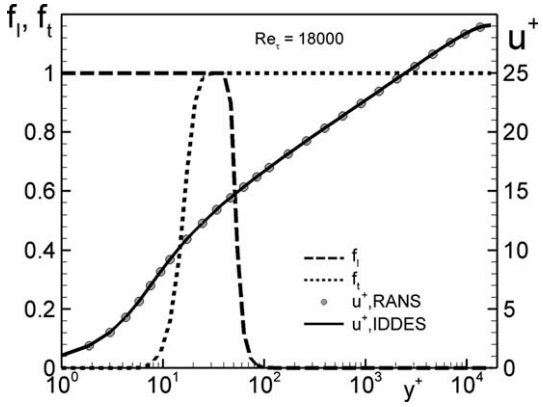


**Fig. 12.** Profiles of the functions $f_t$ and $f_l$ (13) and mean velocity in plane channel computed with MSST-based IDDES initialised by MSST-RANS solution.

RANS solution (recall that in DDES this preservation of RANS in the attached boundary layers was introduced in order to avoid the inaccuracies that result from the activation of the DES limiter in grids that are not fine enough to support a quality LES).

### 3.4. Hydrofoil with trailing edge separation

This is a spanwise homogeneous flow separating from the rear upper side of the asymmetric trailing edge of a hydrofoil (see Fig. 13). The Reynolds number is $2.2 \times 10^6$ based on the chord and $1.01 \times 10^5$ based on the thickness, $h$. The flow is an attractive test of the newly-developed hybrid approach, since it includes both an extended attached boundary layer and a shallow separation bubble, i.e., the features which would cause DDES in its WMLES mode to suffer from LLM, and DES97 to suffer from both LLM and grid-induced separation.

The size of the computational domain is $31h \times 80h \times 0.5h$ in the streamwise, wall normal, and periodic spanwise directions, respectively, and the grid has about 1.5 million nodes with the near-wall $y^+$ value less than 1.0, the streamwise step varying in the range from $0.02h$ up to $0.04h$ (this corresponds to about 10% of the boundary layer thickness), or from ~100 to ~200 in wall units, and the spanwise step equal to $0.02h$($\Delta z^+ = \sim 100$). The simulations are therefore not wall-resolved.

Inflow turbulent content was generated as follows. Parallel to the simulation of the hydrofoil, a similar simulation of flat plate boundary layer was running (in this simulation the triggering of turbulence is performed with the use of the recycling procedure employed by Spalart et al. (2006) for DNS), and the results of this simulation are fed into the inflow boundary of the hydrofoil simulation.

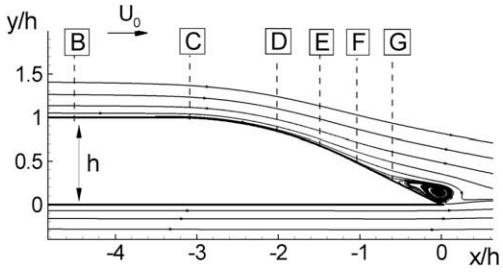


**Fig. 13.** Schematic of the hydrofoil and mean flow streamlines from IDDES. Letters denote positions of sections, where experimental data of Blake, 1975 and full-LES of Wang and Moin (2002) are available (B: $x/h = -4.5$; C: -3.125; D: $-2.125$; E: $-1.625$; F: $-1.125$; G: $-0.625$).

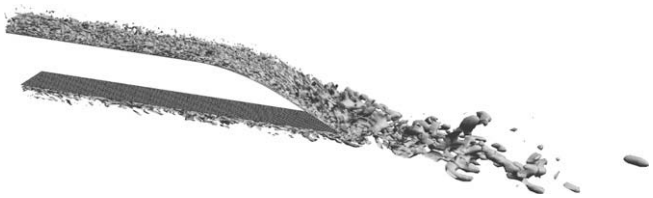

**Fig. 14.** Instantaneous isosurface of swirl from IDDES of hydrofoil flow.

Results of MSST-based IDDES are presented in Figs. 13–15.

Fig. 13, where the streamlines are presented, illustrates the mean flow topology with a trailing edge separation bubble, and Fig. 14 shows the flow visualization in the form of the instantaneous isosurface of "swirl" (imaginary part of the conjugate eigenvalues of the velocity gradient tensor – see Perry and Chong (1987)), which clearly reveals resolved turbulent structures both in the attached boundary layers at the upper and lower hydrofoil surfaces and in its wake. This is obtained thanks to the IDDES performance in WMLES mode in the attached boundary layers and in the separation bubble where the RANS-LES interface is defined by the $f_B$-branch of $\tilde{f}_d$. Finally, Fig. 15 compares results of the present simulation with: the experimental data; the wall-resolved LES of Wang and Moin (2002) carried out with the use of the dynamic SGS model on a C-grid with nearly 7 million nodes; and the hybrid LES-RANS model of Tessicini et al. (2006) with prescribed RANS-LES interface ($y^+ = 60$ in the straight portion of the airfoil) and a grid close to ours. Neither of these simulations can be considered as an absolute reference, but they should bound the numerical/method-related scatter for this arduous problem. Although based on a comparison of skin friction distributions (not shown) IDDES predicts separation somewhat late compared to full LES, results presented in Fig. 15 suggest that, in general, its agreement with the experimental data and the full LES is fairly good both in the attached and separated parts of the boundary layer and also in the wake of the hydrofoil (not shown). This is true not only for the mean streamwise velocity profiles (Fig. 15a) but also for the *rms* of its fluctuations (Fig. 15b). Note that IDDES tangibly surpasses the hybrid model of Tessicini et al., especially in terms of the *rms* prediction in the sections F and G, i.e., slightly upstream of and inside the separation bubble, which may originate in the favourable turbulence-energy level it fosters. The last plot in Fig. 15a shows velocity profiles in the section G predicted by the SA and MSST RANS models. It reveals that both models are noticeably less accurate than the turbulence-resolving approaches.

### 3.5. Backward-facing step flow

This flow is a rather severe test for IDDES, since in this case it must automatically provide three different types of behaviour depending on the flow region. Namely, it should function as a RANS model in the attached boundary layers upstream of the step and on the upper wall of the channel which do not have any "turbulent content", as LES in the separation zone, and, finally, as WMLES in the reattached boundary layer on the step-wall, which inherits "turbulent content" from the upstream separation zone.

As already mentioned, the specific flow we have considered is that studied experimentally by Vogel and Eaton (1985). This is a flow in a plane channel with the step on the lower wall. The Reynolds number based on the step height, $H$, is equal to 28,000 and the channel expansion ratio is 5/4. The incoming boundary-layer thickness is $1.07H$ and it is turbulent. The length of the computational domain is $24H$, with $4H$ upstream and $20H$ downstream of the step. The grid used in the simulations contains 1.5 million nodes total and has appropriate clustering near the walls and in

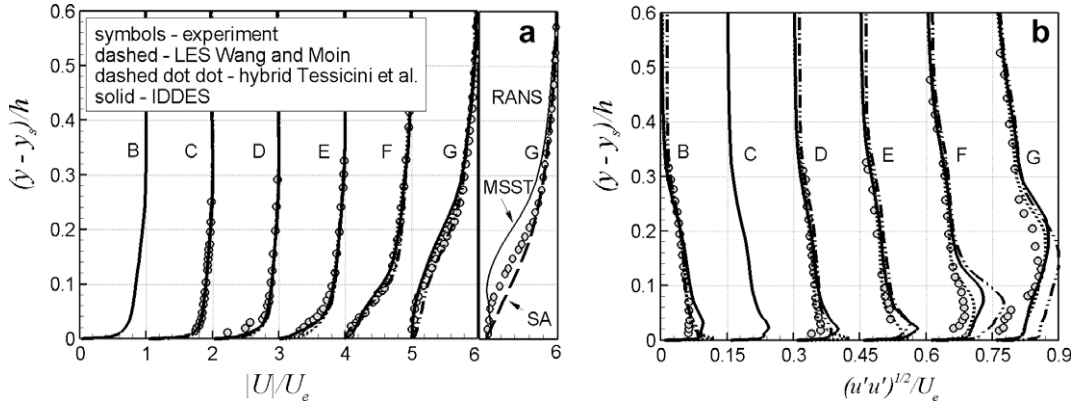


**Fig. 15.** Comparison of streamwise velocity and *rms* of its fluctuations in hydrofoil boundary layer predicted by different simulation approaches. (a) Mean velocity magnitude from IDDES, LES, and hybrid RANS-LES at different cross-sections and from SA and MSST RANS at section G; (b) *rms* from IDDES, LES, and hybrid RANS-LES at different cross-sections.

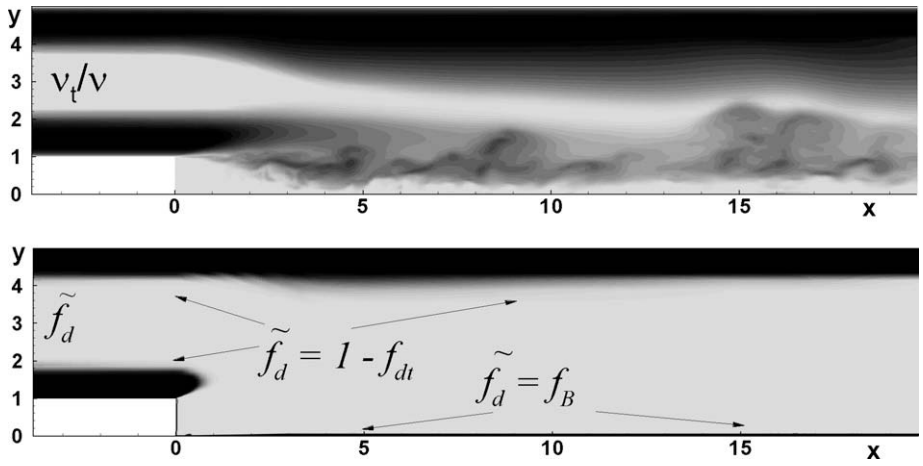


**Fig. 16.** *XY*-cuts of instantaneous fields of eddy viscosity and function $\tilde{f}_d$ from MSST-based IDDES of BFS flow.

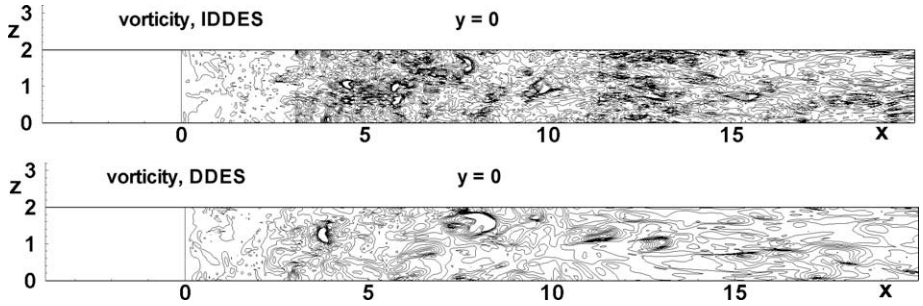


**Fig. 17.** Snapshot of vorticity magnitude on the step wall from MSST-based IDDES and DDES of BFS flow.

the vicinity of the step. It is uniform in the spanwise direction (the span size of the domain is equal to 2 step heights, and the non-dimensional step $\Delta z$ is equal 1/30).

Results of the simulations fully confirm the expected behaviour of both SA- and MSST-based versions of IDDES. As an example, in Fig. 16 we show *XY*-cuts of the instantaneous fields of the eddy viscosity and hybrid function from the simulation with the use of MSST-based IDDES. One can see that in the attached boundary layer approaching the step and in the boundary layer at the upper wall, the $(1 - f_{dt})$-branch of the function $\tilde{f}_d$ is active, i.e., the model is in DDES mode, while at the step-side the $f_B$-branch prevails, which means that in this region the model works as WMLES (the behaviour of $\tilde{f}_d$ in the SA-based IDDES is exactly the same). Moreover, a comparison of the instantaneous vorticity fields on the lower wall of the channel downstream of the step from the simulation with the use of IDDES and DDES presented in Fig. 17 reveals noticeable advantages of IDDES. In the vicinity of this wall IDDES operates in WMLES mode, and, for this reason, provides a better resolution of the fine turbulent structures, which is especially important for the region of recovery of the reattached boundary layer known to be the most challenging for both RANS and DDES. This leads to a more accurate prediction of the mean flow characteristics by both SA- and MSST-based versions of IDDES not only versus the corresponding background RANS models but, more

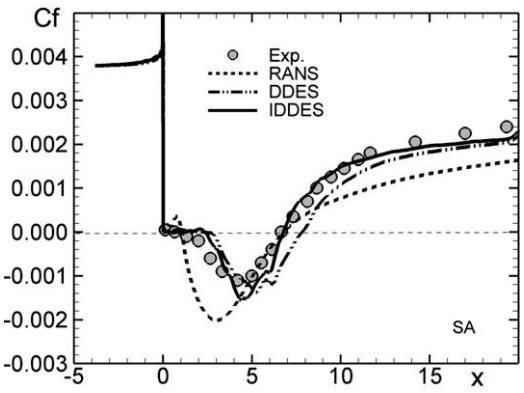


**Fig. 18.** Comparison of mean friction coefficient distributions in BFS flow predicted by RANS, DDES, and IDDES based on SA model with experiment.

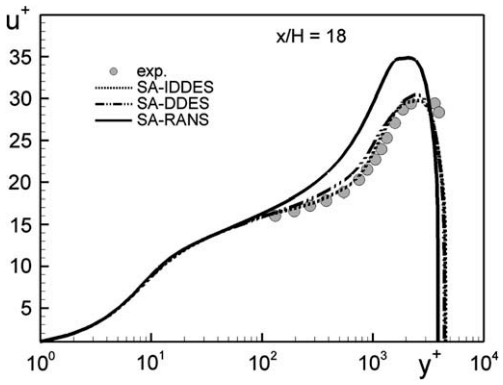


**Fig. 19.** Comparison of mean velocity profiles in recovery region of BFS flow predicted by RANS, DDES, and IDDES based on SA model with experiment.

importantly, versus the corresponding DDES versions as well. This is seen in Figs. 18 and 19, where we compare the skin friction distributions over the step-wall of the channel and mean velocity profiles in the recovery region predicted by the SA-based IDDES and DDES with the experimental data. Quite consistently with the better representation of turbulence, the superiority of IDDES over DDES shows up not only with regard to the prediction of the flow in the recirculation zone downstream of the step, but also in the region of flow recovery after reattachment. Although the skin friction remains somewhat under-predicted past $x = 12$, this may well be explained by the insufficient spanwise domain in the simulation ($2H$, which is slightly less than the boundary-layer thickness) and, also, by the fact that the flow is far from having settled again into a normal zero-pressure-gradient boundary layer, so that a finer grid may be needed for its more accurate representation. Note that for the MSST-based IDDES, the improvement of the flow prediction compared to RANS turns out to be less pronounced than for the SA version, which is not surprising considering the better behaviour of the MSST RANS than that of the SA RANS for a backward-facing step flow (see, e.g., Shur et al., 1995).

## 4. Conclusions

A new hybrid model, IDDES, plausibly combining DDES and WMLES capabilities is proposed. The model is shown to resolve the issue of mismatch between the modelled log layer and the resolved log layer, which has been typical of either DES or DDES use for WMLES. Along with this, IDDES performs just as DES97 and DDES in the natural uses of these approaches (external flows with massive separation) and tangibly surpasses them in the mixed flows with both attached and separated regions (hydrofoil with a trailing edge separation, backward-facing step). Two versions of IDDES, based on the SA and MSST background RANS models, work equally well. They are simple in implementation, cost-free, and appear robust based on a fair set of test cases. The experience base includes the present material, and already independent applications of an earlier version of IDDES (Travin et al., 2006) by Piomelli et al. (2007) and by Mockett et al. (2007), who have been generally satisfied with it. IDDES has not yet been demonstrated for unstructured grids, but WMLES on unstructured grids is far from common, if it has even been achieved at all. The behaviour of IDDES also needs to be verified in grids that are not distributed as smoothly as the present ones, although the backward-facing step shown here does contains needlessly fine regions, linked to the structured character of the grid.

In general, IDDES significantly broadens the application area of (D)DES by permitting the activation of RANS and LES in different flow regions, giving an admittedly intricate but well-balanced and powerful numerical approach to complex turbulent flows at high Reynolds numbers.

## Acknowledgement

Authors from NTS were partially supported by the EC within the research project DESIDER (http://cfd.me.umist.ac.uk/desider) under contract No. AST3-CT-200-502842.

## References

Abe, K., 2005. A hybrid LES/RANS approach using an anisotropy-resolving algebraic turbulence model. International Journal of Heat and Fluid Flow 26, 204–222.
Batten, P., Goldberg, U., Chakravarthy, S., 2002. LNS – an approach towards embedded LES. AIAA Paper 2002-0427.
Batten, P., Chakravarthy, U., Goldberg, S., 2004. Interfacing statistical turbulent closures with large-eddy simulations. AIAA Journal 42 (3), 485–492.
Blake, W.K., 1975. Statistical description of pressure and velocity fields at the trailing edge of a flat structure. DTNSRDC Report 4241, David Taylor Naval Ship R&D Center, Berthesda, MD.
Davidson, L., Billson, M., 2006. Hybrid LES-RANS using synthesized turbulence for forcing in the interface region. International Journal of Heat and Fluid Flow 27, 1028–1042.
Davidson, L., Dahlstrom, S., 2005. Hybrid LES-RANS: an approach to make LES applicable at high Reynolds number. International Journal of Computational Fluid Dynamics 19 (6), 415–427.
Menter, F.R., 1993. Zonal two-equation $k$–$\omega$ turbulence models for aerodynamic flows. AIAA Paper 1993-2906.
Mockett, C., Greschner, B., Knacke, T., Perrion, R., Yan, J., Thiele, F., 2007. Demonstration of improved DES methods for generic and industrial applications. In: Hasse, W., Peng, S.-H. (Eds.), Proceedings of Second Symposium on Hybrid RANS-LES Methods, Corfu, Greece, 17–18 June 2007.
Moser, R.D., Kim, J., Mansour, N.N., 1999. Direct numerical simulation of turbulent channel flow up to $Re_\tau = 590$. Physics of Fluids 11, 943–945.
Nikitin, N., Nicoud, F., Wasistho, B., Squires, K.D., Spalart, P.R., 2000. An approach to wall modeling in large-eddy simulations. Physics of Fluids 12 (7), 1629–1632.
Perry, A.E., Chong, M.S., 1987. A study of eddying motions and flow patterns using critical point concepts. Annual Review of Fluid Mechanics 19, 125–155.
Piomelli, U., Balaras, E., 2002. Wall-layer models for large-eddy simulations. Annual Review of Fluid Mechanics 34, 349–374.
Piomelli, U., Moin, P., Ferziger, J.H., 1988. Model consistency in large-eddy simulation of turbulent channel flows. Physics of Fluids 31, 1884–1894.
Piomelli, U., Radhakrishnan, S., Zhong, L., Li, M., 2007. Wall-layer models for large-eddy simulations of high Reynolds number non-equilibrium flows. In: Palma, J.M.L.M., Lopes, A.S. (Eds.), Advances in Turbulence XI. Springer, Berlin, pp. 47–54.
Reichardt, H., 1951. Vollstandige darstellung der turbulenten geschwindigkeitsverteilung in glatten leitungen. Zeitschrift für Angewandte Mathematik und Mechanik 31, 208–219.
Rogers, S.E., Kwak, D., 1988. An upwind differencing scheme for the time-accurate incompressible Navier–Stokes equations. AIAA Paper 1988-2583-CP.
Schiestel, R., Dejoan, A., 2005. Toward a new partially integrated transport model for coarse grid and unsteady turbulent flow simulation. Theoretical and Computational Fluid Dynamics 18, 443–468.
Shur, M., Strelets, M., Zaikov, L., Gulyaev, A., Kozlov, V., Secundov, A., 1995. Comparative numerical testing of one- and two-equation turbulence models for flows with separation and reattachment. AIAA Paper 1995-0863.

Shur, M., Strelets, P.R., Spalart, M., Travin, A., 1999. Detached-eddy simulation of an airfoil at high angle of attack. In: Rodi, W., Laurence, D. (Eds.), Engineering Turbulence Modelling and Measurements, vol. 4. Elsevier, pp. 669–678.

Spalart, P.R., 2000. Strategies for turbulence modelling and simulations. International Journal of Heat Fluid Flow 21, 252–263.

Spalart, P.R., Allmaras, S.R., 1994. A one-equation turbulence model for aerodynamic flows. La Rech. Aerospatiale 1 (1), 5–21.

Spalart, P.R., Jou, W.-H., Strelets, M., Allmaras, S.R., 1997. Comments on the feasibility of LES for wings, and on a hybrid RANS/LES approach. In: Liu, C., Liu, Z. (Eds.), Advances in LES/DNS, First AFOSR International Conference on DNS/LES. Greyden Press, Louisiana Tech University.

Spalart, P.R., Deck, S., Shur, M.L., Squires, K.D., Strelets, M.Kh., Travin, A.K., 2006. A new version of detached-eddy simulation, resistant to ambiguous grid densities. Theoretical and Computational Fluid Dynamics 20 (3), 181–195.

Spalart, P.R., Strelets, M., Travin, A., 2006. Direct numerical simulation of large-eddy-break-up devices in a boundary layer. International Journal of Heat and Fluid Flow 27, 902–910.

Strelets, M., 2001. Detached eddy simulation of massively separated flows. AIAA Paper 2001-0879.

Swalwell, K.E., 2005. The effect of turbulence on stall of horizontal axis wind turbines. Ph.D. Thesis, Department of Mechanical Engineering, Monash University.

Temmerman, L., Hadziabdic, M., Leschiziner, M.A., Hanjalic, K., 2005. A hybrid two-layer URANS–LES approach for large eddy simulation at high Reynolds numbers. International Journal of Heat and Fluid Flow 26, 173–190.

Tessicini, F., Temmerman, L., Leschziner, M.A., 2006. Approximate near-wall treatments based on zonal RANSLES hybrid methods for LES at high Reynolds numbers. International Journal of Heat and Fluid Flow 27, 789–799.

Travin, A., Shur, M., Strelets, M., Spalart, P.R., 2002. Physical and numerical upgrades in the detached-eddy simulation of complex turbulent flows. In: Friederich, R., Rodi, W. (Eds.), Fluid Mechanics and its Applications. Advances in LES of Complex Flows, Proc. of EUROMECH Colloquium 412, vol. 65. Kluwer, pp. 239–254.

Travin, A., Shur, M., Spalart, P.R., Strelets, M., 2006. Improvement of delayed detached-eddy simulation for LES with wall modelling. In: Wesseling, P., Oñate, E., Périaux, J. (Eds.), Proceedings (CDROM) of the European Conference on Computational Fluid Dynamics ECCOMAS CFD 2006, Egmond aan Zee, The Netherlands.

Vogel, J.C., Eaton, J.K., 1985. Combined heat transfer and fluid dynamic measurements downstream of a backward-facing step. Journal of Heat and Mass Transfer (Transactions on ASME) 107, 922–929.

Wang, M., Moin, P., 2002. Dynamic wall modelling for large-eddy simulation of complex turbulent flows. Physics of Fluids 14, 2043–2051.